



OPEN

Size, separation, structural order, and mass density of molecules packing in water and ice

SUBJECT AREAS:

FLUIDS

INFRARED SPECTROSCOPY

Yongli Huang^{1*}, Xi Zhang^{2,3*}, Zengsheng Ma¹, Wen Li¹, Yichun Zhou¹, Ji Zhou⁴, Weitao Zheng⁵
& Chang Q. Sun^{1,2,3,5}Received
6 September 2013Accepted
7 October 2013Published
21 October 2013Correspondence and
requests for materials
should be addressed to
C.Q.S. (Ecqsun@ntu.
edu.sg)* These authors
contributed equally to
this work.

¹Key Laboratory of Low-Dimensional Materials and Application Technologies (Ministry of Education) and Faculty of Materials, Optoelectronics and Physics, Xiangtan University, Hunan 411105, China, ²NOVITAS, School of Electrical and Electronic Engineering, Nanyang Technological University, Singapore 639798, ³Center for Coordination Bond and Electronic Engineering, College of Materials Science and Engineering, China Jiliang University, Hangzhou 310018, China, ⁴State Key Laboratory of New Ceramics and Fine Processing, Department of Materials Science and Engineering, Tsinghua University, Beijing 100084, China, ⁵School of Materials Science, Jilin University, Changchun 130012, China.

The structural symmetry and molecular separation in water and ice remain uncertain. We present herewith a solution to unifying the density, the structure order and symmetry, the size (H-O length d_H), and the separation ($d_{OO} = d_L + d_H$ or the O:H length d_L) of molecules packing in water and ice in terms of statistic mean. This solution reconciles: i) the d_L and the d_H symmetrization of the O:H-O bond in compressed ice, ii) the d_{OO} relaxation of cooling water and ice and, iii) the d_{OO} expansion of a dimer and between molecules at water surface. With any one of the d_{OO} , the density ρ ($\text{g}\cdot\text{cm}^{-3}$), the d_L , and the d_H , as a known input, one can resolve the rest quantities using this solution that is probing conditions or methods independent. We clarified that: i) liquid water prefers *statistically* the mono-phase of tetrahedrally-coordinated structure with fluctuation, ii) the low-density phase (supersolid phase as it is strongly polarized with even lower density) exists only in regions consisting molecules with fewer than four neighbors and, iii) repulsion between electron pairs on adjacent oxygen atoms dictates the cooperative relaxation of the segmented O:H-O bond, which is responsible for the performance of water and ice.

Water and ice has attracted much attention because of its anomalies pertaining to issues from galaxy to geology, astrophysics, biology, climate, and to our daily lives¹⁻⁷. However, the structure order, the geometric symmetry, the size and the separation between molecules packing in water and ice (H_2O) and their correlation remain yet highly disputed, independent issues despite decades-long intensive investigation. For instances, the separation between adjacent oxygen atoms (d_{OO}) was measured to vary from 2.70 to 3.00 Å⁸⁻²⁰ and the molecular size (the H-O bond length d_H) changes from 0.970 to 1.001 Å²¹. A H_2O molecule demonstrates high *instantaneous* asymmetry with coordination numbers varying from two²² to four or even greater²³. The geometric structure of the weakly-ordered H_2O liquid was interpreted in terms of either the monomial-phase of tetrahedrally-coordinated structures with thermal fluctuation^{2,24-26} or the mixed-phase of low- and high-density fragmentation²⁷⁻²⁹. However, uncertainties in these seemingly independent issues determine jointly the density of water and ice that is macroscopically detectable but the correlation among these quantities is often ignored in consideration. This fact serves as one essential constraint for the solution to the uniqueness of structure order and molecular separation, in terms of statistic expectation, that water molecules prefer. Therefore, these structural and dimensional discrepancies can be resolved simultaneously based on the framework reported in this Letter without needing any assumption or approximation.

Results

Firstly, the sp^3 -orbital hybridization is the unique choice of oxygen upon reacting with atoms of relatively lower electronegativity, irrespective of the structural phase³⁰. As shown in Figure 1a, an oxygen atom ($2s^22p^4$) catches two electrons from neighboring atoms such as hydrogen (H) and metals and then hybridizes its sp orbits with tetrahedrally directional orbits²⁶. In the case of H_2O , one O forms two intramolecular H-O bonds with shared electron pairs and ~ 4.0 eV binding energy²⁶ and fills up the rest two orbits with its nonbonding electron lone pairs “:” to form the intermolecular O:H non-covalent bonds of < 0.1 eV binding energy³¹. The inhomogeneous

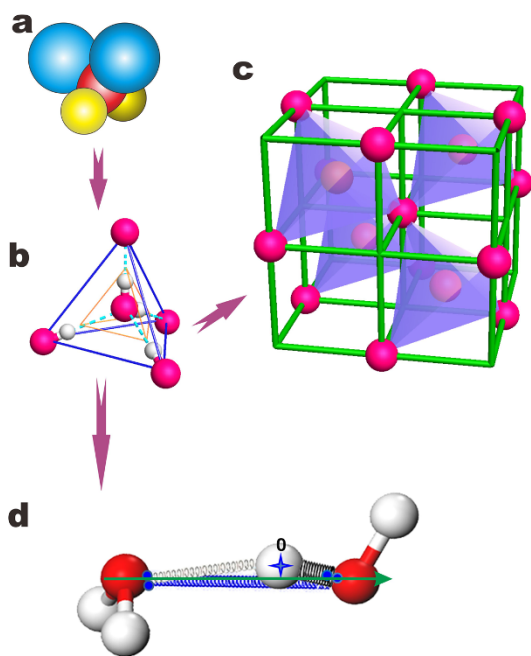


Figure 1 | Sampling procedure for the structure of water and the segmented O:H-O bond. (a) An extension of (a) the sp^3 -hybridized oxygen (red) motif with two nonbonding electron lone pairs (blue) and two bonding electron pairs (yellow) results in (b) an ideal tetrahedron that contains two equivalent H_2O molecules connected by four identical O:H-O bonds of different orientations. The packing of the basic building blocks (b) forms (c) a diamond structure, which ensures the tetrahedral coordination of the central oxygen atom in the coordination origin. Therefore, only four of the eight cubes in (c) are occupied by (b) and the rest four remain empty. (d) The O:H-O bond forms an asymmetric, coupled, H-bridged oscillators whose relaxation in length and energy and the associated local charge distribution determine the physical properties of water and ice^{26,32,35}. Small pairing dots on oxygen represent the electron pairs.

distribution of charge and energy around the central oxygen atom entitles a H_2O molecule only C_{v2} group symmetry except for the rotation and vibration of the molecule. Therefore, an oxygen atom always tends to find four neighbors to form a stable tetrahedron but the nonequivalent bond angles ($\angle H-O-H < 104.5^\circ$ and $\angle H:O:H > 109.5^\circ$) and the repulsion between electron pairs on oxygen^{26,32} refrain the steady tetrahedron from being formed in the liquid phase. The strong fluctuation proceeds more like the motion of a complex pendulum surrounded by four non-bonding lone pairs, because of the O:H bond switching on and off restlessly in a period of sub-picosecond^{2,25,28,29}. Therefore, it would be more realistic and meaningful to consider the statistic expectation of the coordination number, the structure order, and the molecular separation in all phases at question for a long time span rather than seeking for the instantaneous accuracy of a certain independent quantity by taking the snapshot at a quick flash²⁵ for the highly correlated and fluctuating system.

Secondly, the packing order of H_2O molecules follows Pauling's Ice Rule³³ in all phases except for water under extremely high temperature and high pressure³⁴. Despite thermal fluctuation in the O:H non-covalent bond lengths and the $\angle O:H-O$ bond angles, the average separation and the size of molecules will change when the H_2O transits from the strongly-ordered solid phase, to the weakly-ordered liquid phase, and to the disordered amorphous or vapor phase, as the Ice Rule retains. An extension of the Ice Rule results in an ideal tetrahedron, shown in Figure 1b, with higher C_3 group symmetry.

This tetrahedron containing two equivalent H_2O molecules and four identical O:H-O bonds at different orientations forms the basic block building up the bulk water and ice despite fluctuations.

Thirdly, as illustrated in Figure 1c, four of the eight cubes are occupied by the basic $2H_2O$ block tetrahedrally and the rest four cubes are empty, which means that each cube of a^3 volume accommodates only one H_2O molecule on average. With the known mass of a H_2O molecule consisting 8 neutrons, 10 protons, and 10 electrons, $M = (10 \times 1.672621 + 8 \times 1.674927 + 10 \times 0.000911) \times 10^{-27}$ kg and the known density $\rho = M/a^3 = 1$ (gcm^{-3}) at $4^\circ C$ under the atmospheric pressure, this structural order defines immediately and unambiguously the density-dependent molecular separation, d_{OO} , and the next-nearest neighboring distance $\sqrt{2}a$ (unit in \AA),

$$\begin{cases} d_{OO} = \sqrt{3}a/2 = 2.6950\rho^{-1/3} \\ \sqrt{2}a = 4.4001\rho^{-1/3} \end{cases} \quad (1)$$

Finally, the O:H-O bond, in Figure 1d, consists of the longer-and-softer part of the O:H van der Waals bond (d_L) and the shorter-and-stiffer part of the H-O polar-covalent bond (d_H) rather than either of them alone. The O:H-O bond approximates a pair of asymmetric and H-bridged oscillators coupled by Coulomb-repulsion, whose relaxation in length and energy and the associated local charge distribution determine the anomalies of water ice under various stimuli such as compression³², coordination number reduction²⁶, and cooling^{1,7,35}. Under excitation, oxygen atoms dislocate along the O:H-O bond in the same direction but by different amounts with H atom as the coordination origin. The O:H-O interaction in Figure 1d holds statistically true in any phase including amorphous despite the strong fluctuations whose extent is subject to the thermal conditions due to the switching on and off the O:H interactions.

A molecular dynamics (MD) computation has enabled us to decompose the measured volume-pressure $V(P)$ profile of compressed ice^{36,37} into the $d_H(P)$ and the $d_L(P)$ cooperative curves³², see Figure 2. The $d_x(P)$ curves meet at $d_L = d_H = 1.12 \text{ \AA}$ under ~ 59 GPa pressure of ice, which is exactly the measured proton symmetrization of hydrogen bond in ice^{38,39}.

This coincidence indicates that the MD derived $d_x(P)$ relation represents the true cooperativity of the d_L and the d_H bond relaxation. Plotting the $d_L(P)$ against the $d_H(P)$ yields immediately the (projection along the O—O) length cooperativity that is free from probing conditions or probing methods,

$$d_L = 2.5621 \times [1 - 0.0055 \times \exp(d_H/0.2428)] \quad (2)$$

The d_x ($x = L$ and H) value approaches the true bond length with $\sim 1.5\%$ deviation ($1 - \cos(10^\circ) = 0.015$) as the O:H-O angle remains 160° in liquid and greater in solid³⁵. Combining eqs (1) and (2), one is able to scale the size d_H and the separation d_{OO} of H_2O molecules with the given packing order in Figure 1c and the measured density under various conditions. If the d_{OO} or the d_H matches those of direct measurement, the structure order in Figure 1c and eqs (1) and (2) are justified true and unique.

Using eq 1, one can convert, as shown Figure 3a for instance, the measured density $\rho(T)$ profiles of water droplets of different sizes (1.4 and 4.4 nm)^{40,41} as input into the d_{OO} as an output for water at different temperatures. The density transition points change with water droplet size. For droplet of 1.4 nm, the transition is at 205 K, it is at 242 K for 4.4 nm droplet and 258 K for the bulk water³⁵. The droplet size discriminated density transition arises from the specific heat disparity of the O:H- and the H-O within the O:H-O bond. As the droplet size is reduced, the H-O bond becomes shorter and stiffer yet the O:H bond the otherwise²⁶, which shifts the cross points of the two specific heat to temperatures outwardly away from that of the bulk (refer to Ref. 35). The d_{OO} in a water droplet expands additionally in the skin region⁴² but one can only measure its aver-

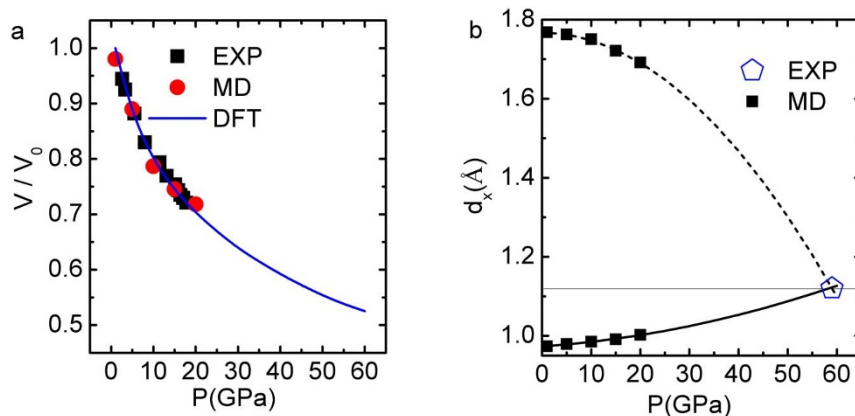


Figure 2 | (a) MD calculation reproduction of the $V(P)$ profile of ice³⁶ with derivatives of the O:H and H-O lengths meeting at $d_H = d_L = 1.12 \text{ \AA}$ under 58.6 GPa compression, which agrees with the measurements of $d_H = d_L = 1.12 \text{ \AA}$ at 59 GPa^{38,39}.

age²⁶. The d_{OO} values of 2.70 Å measured at 25°C and 2.71 Å at -16.8°C ¹⁰ match exactly the conversion of 2.6950 Å that is a projection along the O—O at 4°C. This consistency justifies sufficiently that both eq 1 and the packing order in Figure 1c describe the true situations in both water and ice. Furthermore, the data reported in Ref. 10 is essentially accurate and correct.

Discussion

The non-covalent bond length d_L , molecular size d_H , molecular separation d_{OO} , and the mass density ρ can be obtained by solving the equation with any one of these parameters as a known input,

$$d_L - 2.5621 \times [1 - 0.0055 \times \exp((d_{OO} - d_L)/0.2428)] = 0.$$

Figure 3b shows the decomposition of the d_{OO} into the d_x of water and ice at cooling^{40,41}. The $d_x(T)$ profiles follow the rules of O:H-O bond relaxation^{26,32,35}: i) both oxygen atoms dislocate in the same direction (see inset) along the O:H-O bond by different amounts with respect to the H atom; ii) the longer-and-softer O:H part always relaxes more than the shorter-and-stiffer H-O part does. The cooperativity of the d_x relaxation confirms further that³⁵: i) cooling contraction happens only to the O:H bond in the solid ($T < 205 \text{ K}$ (Data 1) or 241 K (Data 2)) and in the liquid phase ($T > 277 \text{ K}$), which lengthens the H-O bond slightly by inter-electron-pair repulsion, resulting volume contraction; ii) in the freezing transition phase, the process of length relaxation reverses, leading to the O—O length gain and volume expansion at freezing.

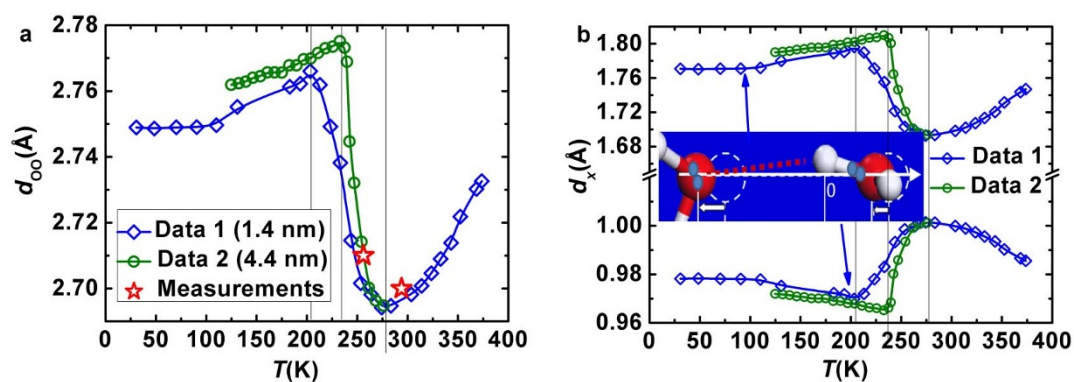


Figure 3 | (a) The $d_{OO} \sim \rho(T)$ profiles (eq 1) of water droplets of different sizes (1.4 and 4.4 nm)^{40,41} match the d_{OO} values measured at 25°C and -16.8°C (Figure S1 and S2 of Supporting Information)¹⁰. (b) The d_H and the d_L (eq 2) agrees with results of MD calculations³⁵. Inset (b) illustrates the cooperative relaxation of the segmented O:H-O bond. One part becomes longer; the other part will be shorter by different amounts due to the inter-electron pair repulsion.

Figure 4 shows the solution consistency to the measured molecular size d_H , molecular separation d_L (or d_{OO}), mass density ρ , and structural order of: i) compressed ice³⁶, ii) cooling water and ice^{40,41}, and, iii) water surface and dimer^{10,19}. The d_H of 1.0004 Å at unity density is within the measured values ranging from 0.970 to 1.001 Å²¹. The d_{OO} values greater than the ideal value of 2.6950 Å at $\rho = 1 \text{ (g}\cdot\text{cm}^{-3}\text{)}$ correspond to the supersolid phase (low-density, LDP) that exists indeed^{27–29} but only presents in the skins of water ice composed of molecules with fewer than four neighbors (Figure 4b)²⁶.

Wilson et al¹⁹ have discovered that the surface d_{OO} expands by 5.9% from 2.801 to 2.965 Å at room temperature. If one considers the shortest distance of 2.70 Å¹⁰ and the longest 2.965 Å¹⁹ of measurements, the surface d_{OO} expands by up to 10%. Furthermore, the volume of water molecules confined in 5.1 and 2.8 nm TiO₂ pores increase by 4 and 7.5%, respectively, with respect to that in the bulk¹³. With a 5–10 Å thick air gap existing in between molecules and the hydrophobic surface⁴⁴, water molecules at the interface exhibit skin vibration attributes⁴⁵ of 3400 cm⁻¹ compared to that of 3200 cm⁻¹ for the bulk water. The separation $d_{OO} = 2.980 \text{ \AA}$ for a dimer is even greater.

In these supersolid regions, molecular under-coordination shortens the d_H and lengthens the d_L , resulting in d_{OO} expansion and polarization because of the inter electron-pair repulsion²⁶. The least density of ice is 0.92, which corresponds to $d_{OO} = 2.695(0.92)^{-1/3} = 2.7710 \text{ \AA}$. However, the density of the supersolid phase is $\rho = (2.695/2.965)^3 = 0.7509 \text{ g}\cdot\text{cm}^{-3}$, which is far lower than the least density of the bulk ice or the maximal density of water (0.75/0.92/1.0), according to eq 1. Considering the limitation of penetration depth in the

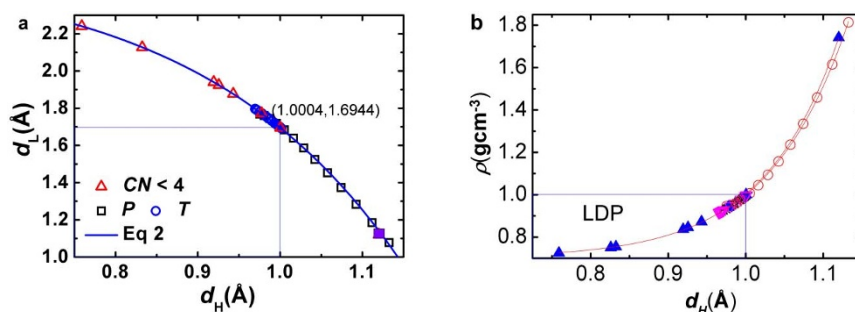


Figure 4 | Accordance of (a) molecular size d_H , molecular separation d_L (or $d_{OO} = d_H + d_L$), (b) mass density ρ , and packing order (see Figure 1c) of H_2O molecules in the situations: (i) ice under compression ($d_H > 1.00 \text{ \AA}$)³⁶, (ii) water ice at cooling ($0.96 < d_H < 1.00 \text{ \AA}$)^{40,41}, and (iii) liquid surface and dimer ($d_H < 1.00 \text{ \AA}$)^{8–10,14–18}. The derived $d_H = 1.0004 \text{ \AA}$ at $\rho = 1$ is within the measurements ranging from 0.970 to 1.001 \AA ²¹. The d_H shorter than 0.96 \AA corresponds to the supersolid phase in regions of molecules having fewer than four coordination neighbors (CN)^{19,20,26}. In such regions, a H_2O molecule shrinks in size and expands in separation because of inter electron-pair repulsion²⁶.

optical reflection measurements of water and ice, all the reported data for the skin are reasonably correct.

The molecular separation $d_{OO} = d_L + d_H$ grows and molecular size d_H shrinks simultaneously at the skins because of the molecular under-coordination²⁶. The H-O bond contraction follows Goldschmidt-Pauling's rule of "atomic coordination number-radius" correlation^{46,47}; the d_{OO} expansion results from the Coulomb repulsion between electron pairs on adjacent oxygen atoms^{26,32}. The skin region, consisting molecules with fewer than four neighbors, forms such an amazing supersolid phase that possesses the attributes of low-density¹⁹, high elasticity⁴⁸, polarized^{49,50}, dielectric instability⁵¹, thermally stable⁵² and hydrophobic^{53,54} with densely entrapped bonding electrons^{55–58}. The timescale for hydrogen-bond switching dynamics at the surface is about three times slower than that in the bulk⁵⁹ because of the strong polarization and high viscosity.

The findings apply to any situations including solid-liquid (water-ice) interface skin as only mass and volume are involved. At the water-hydrophobic surface of different materials, this findings are only valid to the water skin that forms the low-density supersolid state of polarized, depleted, elastic, and thermally stable²⁶. An air gap of $0.5 \sim 1.0 \text{ nm}$ thick presents between the superhydrophobic substrate and water⁴⁴.

The straightforward yet simple solution presented herewith has thus resolved the seemingly independent geometry and dimension uncertainties of water and ice. We may conclude:

- (i) One should focus on the statistic mean of all the factors and their cooperativity involved rather than the instantaneous accuracy of the individual parameter once at a point of time for the strongly fluctuated water system.
- (ii) The size, separation, structural order, and mass density of molecules packing in water and ice are correlated, which is independent of the structural phases of water and ice or the probing conditions.
- (iii) Constrained by the Ice Rule, the d_H and d_L cooperativity, the solution has reconciled measurements of hydrogen-bond length symmetrization of ice under compression, d_{OO} relaxation of water and ice at cooling, and d_{OO} expansion of a water dimer and molecules at water surface.
- (iv) With any one of the molecular separation, mass density, O:H bond length, and H-O distance as a known input, one can determine using this solution unambiguously the rest three parameters and their change with external conditions such as pressure, temperature, and coordination environment.
- (v) The tetrahedrally-coordinated structure could be the unique choice of water and ice despite fluctuations in the d_L and the $\angle O:H-O$ angle due to the non-equivalent $\angle H:O:H$ and $\angle H-O-H$ bond angles and the inter-electron-pair repulsion.

- (vi) The supersolid (low-density) phase indeed exists but only in regions consisting water molecules with fewer than four neighbors. The supersolidity phase forms because of the Goldschmidt-Pauling's rule of H-O bond contraction due to molecular under-coordination and the inter-electron-pair repulsion pertaining to the O:H-O bond.

Methods

The MD calculations were performed using Forcite's package with *ab initio* optimized forcefield Compass27⁶⁰. The Compass27 has been widely used in dealing with the electronic structures and the hydrogen bond network of water and amorphous ices⁶¹ as well as water chains in hydrophobic crystal channels⁶².

1. Medcraft, C. *et al.* Water ice nanoparticles: size and temperature effects on the mid-infrared spectrum. *PCCP* **15**, 3630–3639 (2013).
2. Petkov, V., Ren, Y. & Suchomel, M. Molecular arrangement in water: random but not quite. *J. Phys.: Condens. Matter* **24**, 155102 (2012).
3. Tsai, M. K., Kuo, J. L. & Lu, J. M. The dynamics and spectroscopic fingerprint of hydroxyl radical generation through water dimer ionization: *ab initio* molecular dynamic simulation study. *PCCP* **14**, 13402–13408 (2012).
4. Liu, Y. & Wu, J. Communication: Long-range angular correlations in liquid water. *J. Chem. Phys.* **139**, 041103 (2013).
5. Ostmeier, J. *et al.* Recovery from slow inactivation in K channels is controlled by water molecules. *Nature* **501**, 121–124 (2013).
6. Gierszal, K. P. *et al.* π -Hydrogen Bonding in Liquid Water. *J. Phys. Chem. Lett.* **2**, 2930–2933 (2011).
7. Medcraft, C. *et al.* Size and temperature dependence in the far-IR spectra of water ice particles. *Astrophys. J.* **758**, 17 (2012).
8. Skinner, L. B. *et al.* Benchmark oxygen-oxygen pair-distribution function of ambient water from x-ray diffraction measurements with a wide Q-range. *J. Chem. Phys.* **138**, 074506 (2013).
9. Wikfeldt, K. T. *et al.* Oxygen-oxygen correlations in liquid water: Addressing the discrepancy between diffraction and extended x-ray absorption fine-structure using a novel multiple-data set fitting technique. *J. Chem. Phys.* **132**, 104513 (2010).
10. Bergmann, U. *et al.* Nearest-neighbor oxygen distances in liquid water and ice observed by x-ray Raman based extended x-ray absorption fine structure. *J. Chem. Phys.* **127**, 174504 (2007).
11. Morgan, J. & Warren, B. E. X-ray analysis of the structure of water. *J. Chem. Phys.* **6**, 666–673 (1938).
12. Naslund, L. A. *et al.* X-ray absorption spectroscopy study of the hydrogen bond network in the bulk water of aqueous solutions. *J. Phys. Chem. A* **109**, 5995–6002 (2005).
13. Orgel, L. The hydrogen bond. *Rev. Mod. Phys.* **31**, 100–102 (1959).
14. Wilson, K. R. *et al.* X-ray spectroscopy of liquid water microjets. *J. Phys. Chem. B* **105**, 3346–3349 (2001).
15. Narten, A. H., Thiessen, W. E. & Blum, L. Atom pair distribution functions of liquid water at 25°C from neutron diffraction. *Science* **217**, 1033–1034 (1982).
16. Fu, L., Bienenstock, A. & Brennan, S. X-ray study of the structure of liquid water. *J. Chem. Phys.* **131**, 234702 (2009).
17. Kuo, J. L., Klein, M. L. & Kuhs, W. F. The effect of proton disorder on the structure of ice-Ih: A theoretical study. *J. Chem. Phys.* **123**, 134505 (2005).
18. Soper, A. K. Joint structure refinement of x-ray and neutron diffraction data on disordered materials: application to liquid water. *J. Phys. Condens. Matter* **19**, 335206 (2007).



19. Wilson, K. R. *et al.* Surface relaxation in liquid water and methanol studied by x-ray absorption spectroscopy. *J. Chem. Phys.* **117**, 7738–7744 (2002).
20. Liu, K., Cruzan, J. D. & Saykally, R. J. Water clusters. *Science* **271**, 929–933 (1996).
21. Hakala, M. *et al.* Intra- and intermolecular effects in the Compton profile of water. *Phys. Rev. B* **73**, 035432 (2006).
22. Wernet, P. *et al.* The Structure of the first coordination shell in liquid water. *Science* **304**, 995–999 (2004).
23. Soper, A. K. Recent water myths. *Pure Appl. Chem.* **82**, 1855–1867 (2010).
24. Head-Gordon, T. & Johnson, M. E. Tetrahedral structure or chains for liquid water. *PNAS* **103**, 7973–7977 (2006).
25. Kuhne, T. D. & Khaliullin, R. Z. Electronic signature of the instantaneous asymmetry in the first coordination shell of liquid water. *Nat. Commun.* **4**, 1450 (2013).
26. Sun, C. Q. *et al.* Density, elasticity, and stability anomalies of water molecules with fewer than four neighbors. *J. Phys. Chem. Lett.* **4**, 2565–2570 (2013).
27. Huang, C. *et al.* The inhomogeneous structure of water at ambient conditions. *PNAS* **106**, 15214–15218 (2009).
28. Wernet, P. *et al.* The structure of the first coordination shell in liquid water. *Science* **304**, 995–999 (2004).
29. Nilsson, A., Huang, C. & Pettersson, L. G. M. Fluctuations in ambient water. *J. Mol. Liq.* **176**, 2–16 (2012).
30. Sun, C. Q. Oxidation electronics: bond-band-barrier correlation and its applications. *Prog. Mater. Sci.* **48**, 521–685 (2003).
31. Zhao, M. *et al.* Atomistic origin, temperature dependence, and responsibilities of surface energetics: An extended broken-bond rule. *Phys. Rev. B* **75**, 085427 (2007).
32. Sun, C. Q., Zhang, X. & Zheng, W. T. Hidden force opposing ice compression. *Chem. Sci.* **3**, 1455–1460 (2012).
33. Pauling, L. The structure and entropy of ice and of other crystals with some randomness of atomic arrangement. *J. Am. Chem. Soc.* **57**, 2680–2684 (1935).
34. Wang, Y. *et al.* High pressure partially ionic phase of water ice. *Nat. Commun.* **2**, 563 (2011).
35. Sun, C. Q. *et al.* Density and phonon-stiffness anomalies of water and ice in the full temperature range. *J. Phys. Chem. Lett.* **4**, 3238–3244 (2013).
36. Yoshimura, Y. *et al.* High-pressure x-ray diffraction and Raman spectroscopy of ice VIII. *J. Chem. Phys.* **124**, 024502 (2006).
37. Sugimura, E. *et al.* Compression of H₂O ice to 126 GPa and implications for hydrogen-bond symmetrization: Synchrotron x-ray diffraction measurements and density-functional calculations. *Phys. Rev. B* **77**, 214103 (2008).
38. Benoit, M., Marx, D. & Parrinello, M. Tunnelling and zero-point motion in high-pressure ice. *Nature* **392**, 258–261 (1998).
39. Goncharov, A. F., Struzhkin, V. V., Mao, H.-k. & Hemley, R. J. Raman spectroscopy of dense H₂O and the transition to symmetric hydrogen bonds. *Phys. Rev. Lett.* **83**, 1998–2001 (1999).
40. Mallamace, F. *et al.* The anomalous behavior of the density of water in the range 30 K < T < 373 K. *PNAS* **104**, 18387–18391 (2007).
41. Erko, M. *et al.* Density minimum of confined water at low temperatures: a combined study by small-angle scattering of X-rays and neutrons. *PCCP* **14**, 3852–3858 (2012).
42. Sulpizi, M., Salanne, M., Sprik, M. & Gaigeot, M.-P. Vibrational sum frequency generation spectroscopy of the water liquid–vapor interface from density functional theory-based molecular dynamics simulations. *J. Phys. Chem. Lett.* **4**, 83–87 (2013).
43. Solveyra, E. G. *et al.* Structure, Dynamics, and Phase Behavior of Water in TiO₂ Nanopores. *J. Chem. Phys. C* **117**, 3330–3342 (2013).
44. Uysal, A. *et al.* What x rays can tell us about the interfacial profile of water near hydrophobic surfaces. *Phys. Rev. B* **88**, 035431 (2013).
45. Kasuya, M. *et al.* Characterization of Water confined between Silica surfaces using the resonance shear measurement. *J. Phys. Chem. C* **117**, 13540–13546 (2013).
46. Goldschmidt, V. M. Crystal structure and chemical correlation. *Ber Deut Chem Ges* **60**, 1263–1296 (1927).
47. Pauling, L. Atomic radii and interatomic distances in metals. *J. Am. Chem. Soc.* **69**, 542–553 (1947).
48. Kahan, T. F., Reid, J. P. & Donaldson, D. J. Spectroscopic probes of the quasi-liquid layer on ice. *J. Phys. Chem. A* **111**, 11006–11012 (2007).
49. Siefertmann, K. R. *et al.* Binding energies, lifetimes and implications of bulk and interface solvated electrons in water. *Nat. Chem.* **2**, 274–279 (2010).
50. Ishiyama, T., Takahashi, H. & Morita, A. Origin of vibrational spectroscopic response at ice surface. *J. Phys. Chem. Lett.* **3**, 3001–3006 (2012).
51. Zhang, C., Gygi, F. & Galli, G. Strongly anisotropic dielectric relaxation of water at the nanoscale. *J. Phys. Chem. Lett.* **4**, 2477–2481 (2013).
52. Qiu, H. & Guo, W. Electromelting of confined monolayer ice. *Phys. Rev. Lett.* **110**, 195701 (2013).
53. Wang, C. *et al.* Stable liquid water droplet on a water monolayer formed at room temperature on ionic model substrates. *Phys. Rev. Lett.* **103**, 137801–137804 (2009).
54. James, M. *et al.* Nanoscale condensation of water on self-assembled monolayers. *Soft Matter* **7**, 5309–5318 (2011).
55. Winter, B. *et al.* Hydrogen bonds in liquid water studied by photoelectron spectroscopy. *J. Chem. Phys.* **126**, 124504 (2007).
56. Abu-Samha, M. *et al.* The local structure of small water clusters: imprints on the core-level photoelectron spectrum. *J. Phys. B* **42**, 055201 (2009).
57. Nishizawa, K. *et al.* High-resolution soft X-ray photoelectron spectroscopy of liquid water. *PCCP* **13**, 413–417 (2011).
58. Vacha, R. *et al.* Charge transfer between water molecules as the possible origin of the observed charging at the surface of pure water. *J. Phys. Chem. Lett.* **3**, 107–111 (2012).
59. Ni, Y., Gruenbaum, S. M. & Skinner, J. L. Slow hydrogen-bond switching dynamics at the water surface revealed by theoretical two-dimensional sum-frequency spectroscopy. *PNAS* **110**, 1992–1998 (2013).
60. Sun, H. COMPASS: An ab initio force-field optimized for condensed-phase applications: Overview with details on alkane and benzene compounds. *J. Phys. Chem. B* **102**, 7338–7364 (1998).
61. He, C., Lian, J. S. & Jiang, Q. Electronic structures and hydrogen bond network of ambient water and amorphous ices. *Chem. Phys. Lett.* **437**, 45–49 (2007).
62. Natarajan, R., Charmant, J. P. H., Orpen, A. G. & Davis, A. P. Water chains in hydrophobic crystal channels: Nanoporous materials as supramolecular analogues of carbon nanotubes. *Angew. Chem. Int. Ed.* **49**, 5125–5129 (2010).

Acknowledgements

Critical reading by Yi Sun and financial support received from NSF (Nos.: 21273191, 1033003, and 90922025) China are gratefully acknowledged.

Author contributions

X.Z. and Y.H. contribute equally in computations. Z.M. and W.L. initiated the topic of research and prepared figures. Y.Z., J.Z. and W.Z. involved explanations. C.S. wrote the manuscript. All authors reviewed the manuscript.

Additional information

Supplementary information accompanies this paper at <http://www.nature.com/scientificreports>

Competing financial interests: The authors declare no competing financial interests.

How to cite this article: Huang, Y.L. *et al.* Size, separation, structural order, and mass density of molecules packing in water and ice. *Sci. Rep.* **3**, 3005; DOI:10.1038/srep03005 (2013).



This work is licensed under a Creative Commons Attribution 3.0 Unported license. To view a copy of this license, visit <http://creativecommons.org/licenses/by/3.0>